Available online at www.sciencedirect.com
ScienceDirect
Journal of the European Ceramic Society 31 (2011) 989–998
www.elsevier.com/locate/jeurceramsoc

Original Article

Ceramics from blast furnace slag, kaolin and quartz

Emilia Karamanova, Georgi Avdeev, Alexander Karamanov *

Institute of Physical Chemistry, Bulgarian Academy of Sciences, Acad. G. Bonchev Str. Block 11, 1113 Sofia, Bulgaria

Received 23 September 2010; received in revised form 27 December 2010; accepted 10 January 2011
Available online 26 January 2011

Abstract

Three new ceramic batches with no traditional fluxes and 30, 50 and 70 wt.% blast furnace slag were studied. The processes of phase formation and densification were estimated in non-isothermal conditions by differential thermal analysis and dilatometry, respectively. After that the degrees of sintering, obtained after heat-treatment at different temperatures and times, were evaluated measuring the variations of linear shrinkage and water absorption. The structures of final materials and their phase compositions were studied with scanning electron microscopy, pycnometry and X-ray diffraction. Mechanical properties of the final ceramics were also measured.

The obtained ceramics are characterized with a narrow sintering interval at 1200–1220 °C and good degrees of densification. Due to the formation of pyroxene and anorthite solid solution the new materials show high crystallinity. As a result, the measured bending strength and hardness surpass the values of traditional building and tiling materials.

Keywords: Industrial wastes; Ceramics; Sintering; Structure; Properties

1. Introduction

The world production of building and tiling ceramics requires huge amounts of natural raw materials, which until now mainly belong to the system clay–silica–feldspar. Nevertheless, many works demonstrate the possibility for a successful substitution of these "traditional" raw materials by other natural resources as zeolites,[1] volcanic rocks[2,3] and others.[4]

Another extensively studied possibility is the usage of different industrial wastes. This idea has a double environmental effect: at once it can resolve problems with the storage of some industrial wastes and with the mining of traditional ceramic raw materials.

A part of these studies is related to the substitution of feldspars with different waste glasses. Promising results were obtained with waste glass cullet[5–8] and CRT glasses.[9,10] These glass compositions are characterized by lower viscosities than the initial feldspars melts in ceramics, which decreases the sintering temperature and accelerates the dissolution of the quartz phase. As a result, in order to obtain sintering behaviour and mechanical characteristics similar to the plant compositions, the feldspars are substituted only partially. It was shown that the optimal amount of replacement with waste glasses in stoneware porcelains is in the range of 5–15 wt.%.[8–10] At higher percentages of glass addition the closed porosity in final samples increases and their mechanical properties decrease.

Other works examine the possibility to use industrial streams as blast furnace slag,[10–14] MSW ashes,[15,16] other fly ashes[17–20] and different sludge.[5,21,22] In most cases, these residues are used as inert or plastic materials and the sintering process is related mainly to presence of traditional ceramic fluxes in batches. However, if the sintering temperature is higher or/and the melting temperature of used residue is lower, the waste product also can start to melt, which drastically changes the sintering behaviour, the phase composition and the structure of final ceramic.

The aim of present work is to demonstrate that cheap ceramics with good mechanical characteristics can be obtained at a relatively low firing temperature by using high amount of an industrial waste. In the study three new ceramic compositions, containing no feldspar and 30, 50 and 70 percentages of granulated blast furnace slag (BFS), are studied. Some peculiarities of the phase formations and the structure of ceramics are presented and discussed.

* Corresponding author. Tel.: +359 2 8723951.
E-mail address: karama@ipc.bas.bg (A. Karamanov).

0955-2219/$ – see front matter © 2011 Elsevier Ltd. All rights reserved.
doi:10.1016/j.jeurceramsoc.2011.01.006

Table 1
Batch compositions of studied ceramics (wt.%).

Batch	Slag	Kaolin	Sand
S-30	30	30	40
S-50	50	30	20
S-70	70	30	–

2. Experimental procedure

Three batches with 30, 50 and 70 wt.% granulated blast furnace slag (labelled S-30, S-50 and S-70, respectively), which compositions are shown in Table 1, were studied. In order to have similar plasticity the batches contain a constant amount of 30 wt.% kaolin, while different amounts of quartz were added as an inert material.

All raw materials were milled and sieved below 63 μm. Initial mixes with 6 wt.% water content were prepared, homogenized and granulated through 315 μm sieve. Then "green" samples with initial size of 50 mm × 3 mm × 4 mm were obtained by uniaxial pressing at 50 MPa.

The chemical compositions of the used materials and ceramics were evaluated by XRF analysis (Spectro Xepos). The thermal behaviour of initial raw materials and ceramic batches were evaluated by DTA technique (Linseiz L81) using 100 mg powder samples at heating rate of 10 °C/min. The sintering trends were studied by differential dilatometer (Netzsch 402 ED) at 10 °C/min by means of 4 mm × 4 mm × 8 mm specimens.

Samples of each composition were heat-treated for 30 min at different temperatures at heating and cooling rates of 10 °C/min using a laboratory furnace with silit heaters (Nabertherm). The degree of densification of obtained specimens was estimated by the linear shrinkage, $\Delta L/L_0$, and the water absorption, W, measured after 3 h boiling in distillate water and cooling to room temperature.

The apparent, ρ_a, skeleton, ρ_s, and absolute, ρ_{as}, densities of some samples were determined and the results were used to evaluate total, P_T, closed, P_C, and open P_O porosity:

$$P_T = 100 \times \frac{\rho_{as} - \rho_a}{\rho_{as}}, \qquad P_C = 100 \times \frac{\rho_{as} - \rho_s}{\rho_{as}},$$

$$P_O = 100 \times \frac{\rho_s - \rho_a}{\rho_{as}}$$

ρ_a was estimated by a precise micrometer while ρ_s and ρ_{as} by gas (Ar) pycnometer (AccyPy1330, Micromeritics) before and after crashing and milling the samples below 26 μm, respectively.

The phase compositions of samples, heat-treated at different temperature temperature, were characterized by X-ray diffraction analysis (Philips PW1830). The structure and morphology of the new ceramics were observed by scanning electron microscopy (Philips XL30CP) after Au metallization.

Finally, the bending strength and the Vickers hardness were determined. The bending strength was measured using series of 5 samples by the three point method (with external distance of 40 mm and a speed of 0.2 mm/min). The Vickers hardness was estimated after polishing and 3 indentations on each sample at load of 10 kg.

Table 2
Chemical compositions of raw materials and final ceramics.

Oxides	Slag	Kaolin	Sand	S-70	S-50	S-30
SiO_2	39.9	52.6	99.6	45.2	57.8	70.4
Al_2O_3	9.3	33.2	0.2	17.0	15.1	13.2
Fe_2O_3	1.2	0.4	0.1	1.0	0.8	0.5
CaO	34.9	0.2	–	25.2	18.1	10.8
MgO	8.1	–	–	5.8	4.2	2.5
CuO	0.9	–	–	0.7	0.5	0.3
BaO	1.2	–	–	0.9	0.6	0.4
MnO	2.8	–	–	2.0	1.4	0.9
K_2O	1.4	0.3	–	1.1	0.8	0.5
Na_2O	0.2	–	–	0.1	0.1	0.1
SO_3	1.2	–	–	0.9	0.7	0.4
LOI	0.2	13.1	–	–	–	–

3. Results and discussions

3.1. Sintering

The chemical analysis of used slag, kaolin, sand and the resulting ceramics are reported in Table 2. The kaolin and sand are pure raw materials, selected in order to simplify the batches and their examination, while the composition of granulated blast furnace slag is typical for this kind of industrial wastes. It is evident that the compositions of new materials are totally different from ones of the traditional ceramics; even more, S-70 and S-50 are similar to some of the glass-ceramics obtained by vitrification of industrial wastes.[23,24]

The initial slag (labelled S) and the studied ceramics may be satisfactorily expressed thought four component SiO_2–Al_2O_3–CaO–MgO phase diagrams.[25] Fig. 1 shows the SiO_2–CaO–MgO graph at a constant amount of 15 wt.% Al_2O_3, together with recalculated compositions of the used slag and the studied ceramics. It appears that S has a mellelite–gehlenite

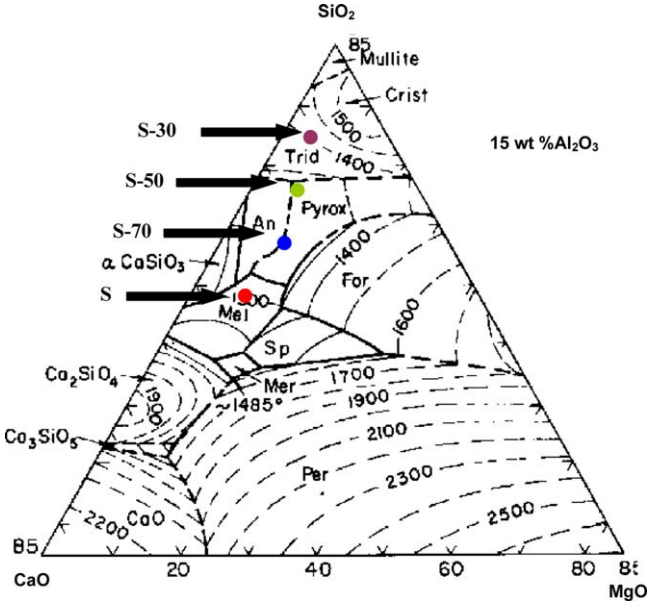

Fig. 1. Phase diagram of SiO_2–Al_2O_3–CaO–MgO and the compositions of used slag and studied ceramics.[25]

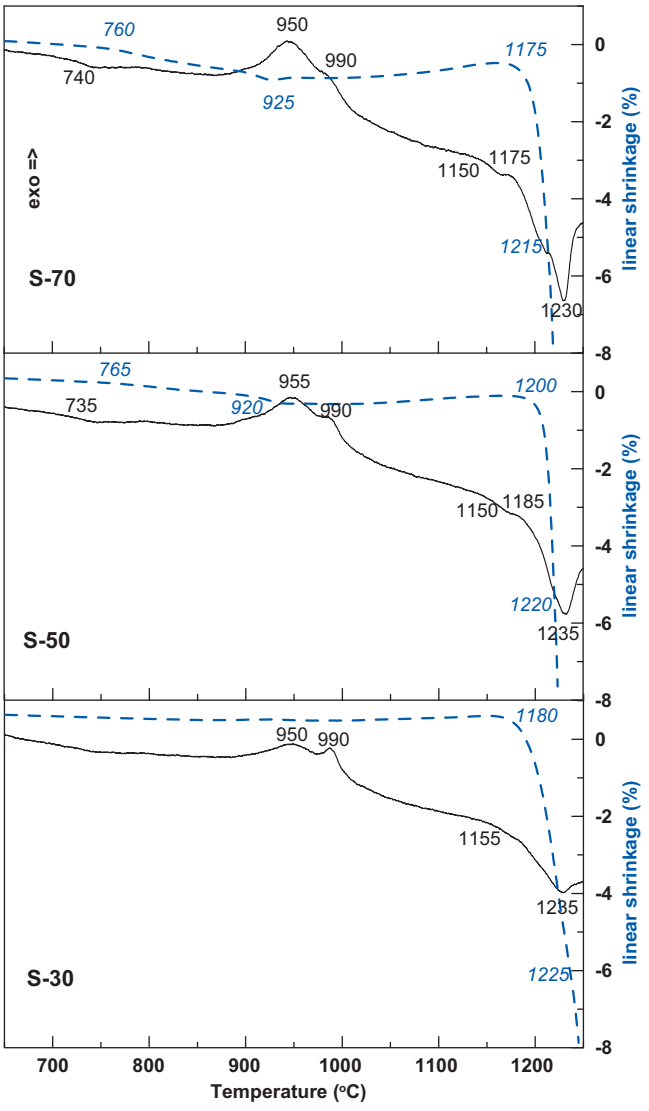

Fig. 2. DTA and dilatometic plots of composition S-30, S-50 and S-70.

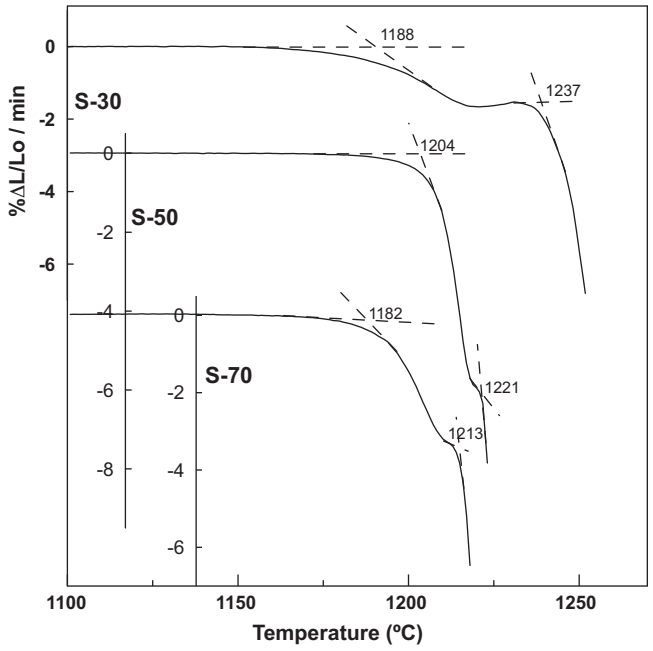

Fig. 3. Shrinkage rates of compositions S-30, S-50 and S-70 in the range of 1100–1250 °C.

composition, while S-70 and S-50 lie between the crystallization fields of anorthite and pyroxene; S-30 is located in the field of SiO_2 phases.

The thermal behaviour of the raw materials was studied by TG-DTA.[26] The kaolin shows a typical dehydratation endotherm at 560 °C and an exotherm at 990 °C because of transformations of metakaolinite in amorphous silica and gamma Al_2O_3, while the sand presents only a low-intensity endo-effect at 570 °C, corresponding to the transformation α into β quartz. The S traces highlight a glass transition at about 730 °C, followed by a crystallization exo-effect with peak temperature at 950 °C and melting endotherm with onset at 1135 °C and peak temperature at 1185 °C. XRD analysis of slag samples, heat-treated for 30 min at 850 °C and 950 °C, elucidate an amorphous structure and formation of gehlenite solid solutions, respectively.

The DTA results (solid line) of S-30, S-50 and S-70 batches, together with the corresponding dilatometric sintering curves (trashed line), in the interval 600–1300 °C are plotted in Fig. 2.

The DTA traces show glass transition temperatures at about 730–740 °C and crystallization exotherms at about 950 °C, which intensities increase with the amount of slag in batches. At the same time, the exotherms at 990 °C, due to metacaolinite transformation, are similar in the three samples. In the interval 1000–1150 °C no effects are presented, which elucidate the lack of intensive solid state reactions between the components.

At higher temperatures different melting endotherms, which intensity increases with the slag amount in batches, are observed. In the three compositions the onset temperatures are at about 1150 °C (i.e. as one in the slag), while the temperatures of melting peaks occur at 1230–1235 °C (i.e. 50–60 °C higher temperatures than one in the slag). In S-50 and S-70 new exo-effects are observed at about 1180–1190 °C, which can be related to recrystallization processes, starting during the melting of gehlenite from slag. The melting of newly formed crystal phases begins at 1210–1220 °C.

The dilatometric curves in interval 750–1000 °C present no variations in S-30, 0.4% shrinkage in S-50 and about 1% shrinkage in S-70, which is related to some sintering taking place between glass transition and crystallization temperatures of the amorphous slag. The actual densification process, which leads to 4–6% shrinkage, is observed in the interval 1180–1230 °C. At higher temperatures starts deformation of the samples.

Fig. 3 demonstrates the sintering rates (i.e. the shrinkage derivates) in the high temperature interval. Here the sintering rate is presented as percentage linear shrinkage ($\Delta L/L_0$), per a minute sintering time. The densification in S-30, S-50 and S-70 starts at about 1190, 1200 and 1180 °C, respectively, while the beginning of deformation occurs at about 1240, 1220 and 1210 °C. The composition S-30 is characterized by the lowest sintering rate of ~2% ($\Delta L/L_0$)/min and the largest sintering interval of about 50 °C. Composition S-50 (notwith-

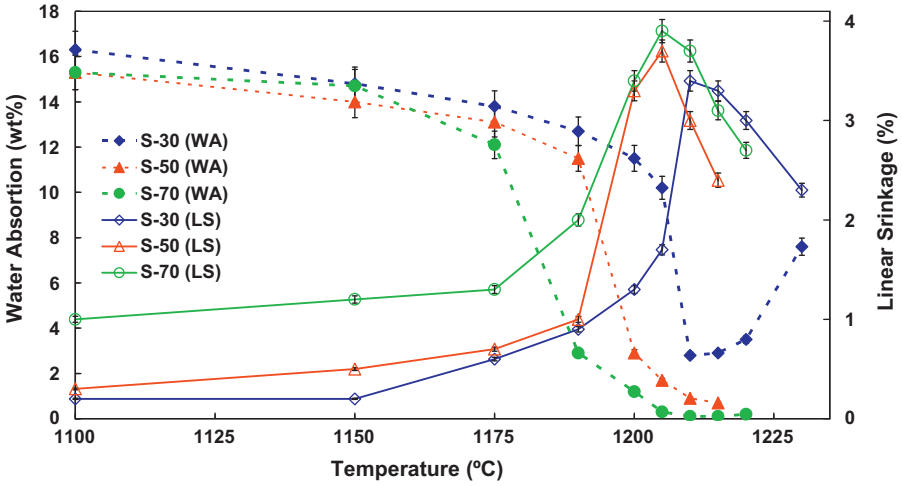

Fig. 4. Linear shrinkage and water absorption after 30 min holding at different temperatures.

standing of inferior slag amount in comparison with S-70) shows the highest sintering rate of about 6% $(\Delta L/L_0)$/min and very narrow densification interval of 15–20 °C. In S-70 the sintering rate is ∼3.5% $(\Delta L/L_0)$/min and the sintering interval is about 30 °C.

These results highlight that only compositions as S-30 and S-70 might be interesting from a technological point of view, while in ceramic S-50 is difficult to control the sintering process and to avoid the deformation. For a comparison, in an identical dilatometric study with a commercial stoneware porcelain[9] the values of the sintering interval and the maximum sintering rate was estimated as ∼150 °C and ∼1.5% $(\Delta L/L_0)$/min, respectively.

The densification behaviour of the three ceramics were confirmed by the values of linear shrinkage and water absorption obtained after 30 min heat-treatment at different temperatures, which are summarised in Fig. 4. The plots demonstrate that the sintering processes start at 1190 °C in S-50 and S-70 and at 1200 °C in S-30, while the beginning of overfiring is observed at 1220–1230 °C. At 1210 °C ceramic S-70 is characterized by zero water absorption, W in S-50 is at about 1%, while in S-30 significant open porosity remains. The shrinkage at 1210 °C for all samples is in the range of 3.5–4%. Then, due to overfiring, in all ceramics $\Delta L/L_0$ decreases; the porosity in S-70 and S-50 remains closed, while in S-30 an increase of the open porosity is observed.

The XRD spectra of new ceramics (30 min at 1210 °C) are plotted in Fig. 5. The sample S-30 shows mainly quartz, together with anorthite and traces of pyroxene and cristobalite. The spectrum of S-50 also indicates some unreacted quartz, but the main phases become anorthite and pyroxene. S-70 shows the highest crystallinity (i.e. lowest intensity of the amorphous halo), which can be related to the significant increase of the pyroxenes.

These XRD results are in a very good agreement with the phase diagram (see Fig. 1). However, they do not explain the reactions, taking place during the heat-treatment, as well as the differences in the structures of studied compositions. In addition, the high crystallinity of sample S-70 is in apparent contradiction with its good sinterability and zero water absorption. For these reasons additional sintering experiments and XRD analysis were carried out with compositions S-30 and S-70.

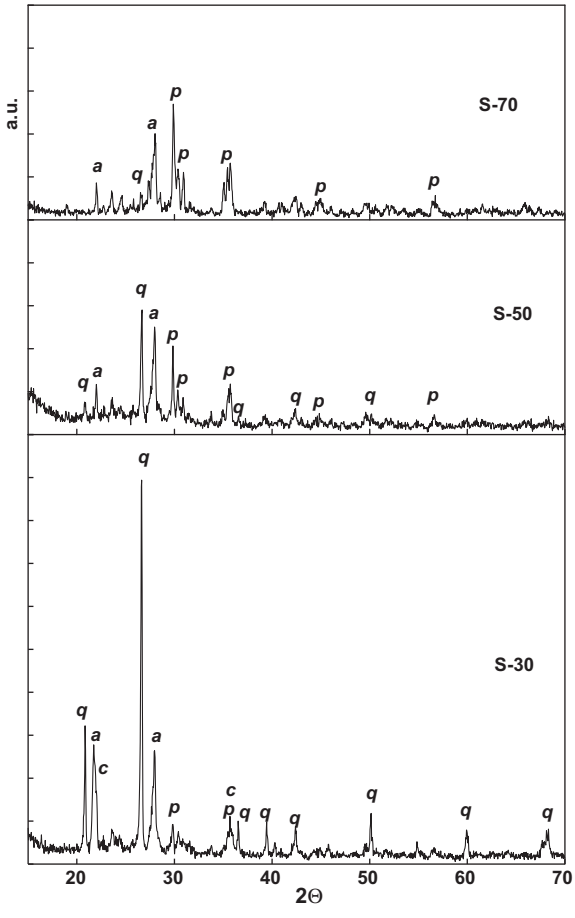

Fig. 5. XRD spectra of final ceramics after 30 min holding at 1210 °C (q, quartz; a, anorthite; p, pyroxene; c, cristobalite).

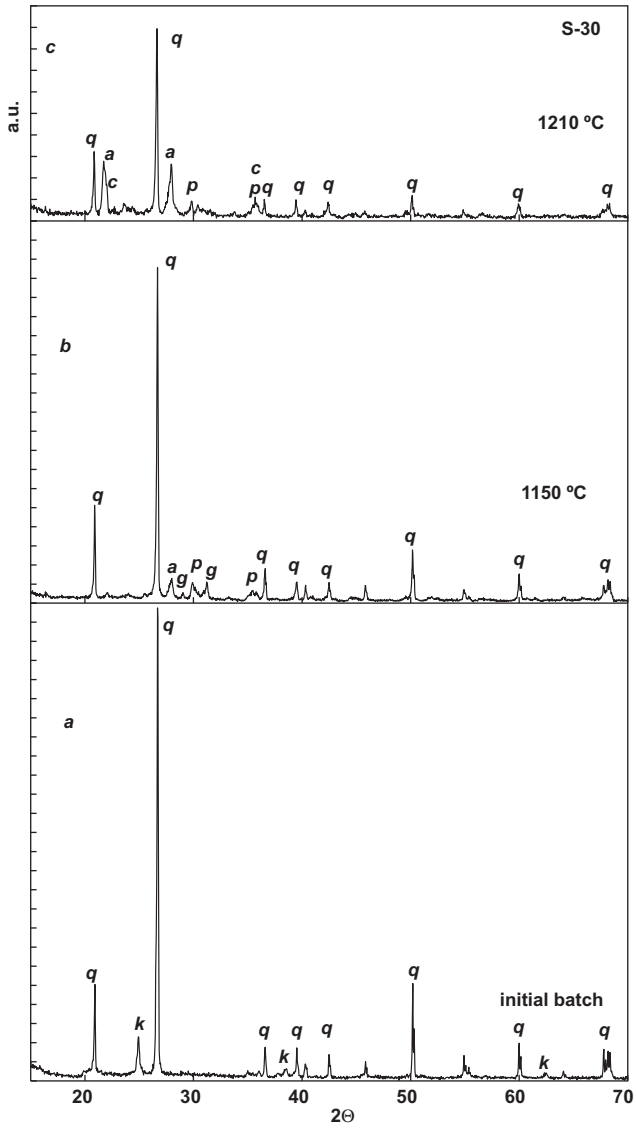

Fig. 6. XRD spectra of S-30 compositions after 30 min holding at different temperatures (q, quartz; a, anorthite; p, pyroxene; c, cristobalite; g, gehlenite; k, kailonite).

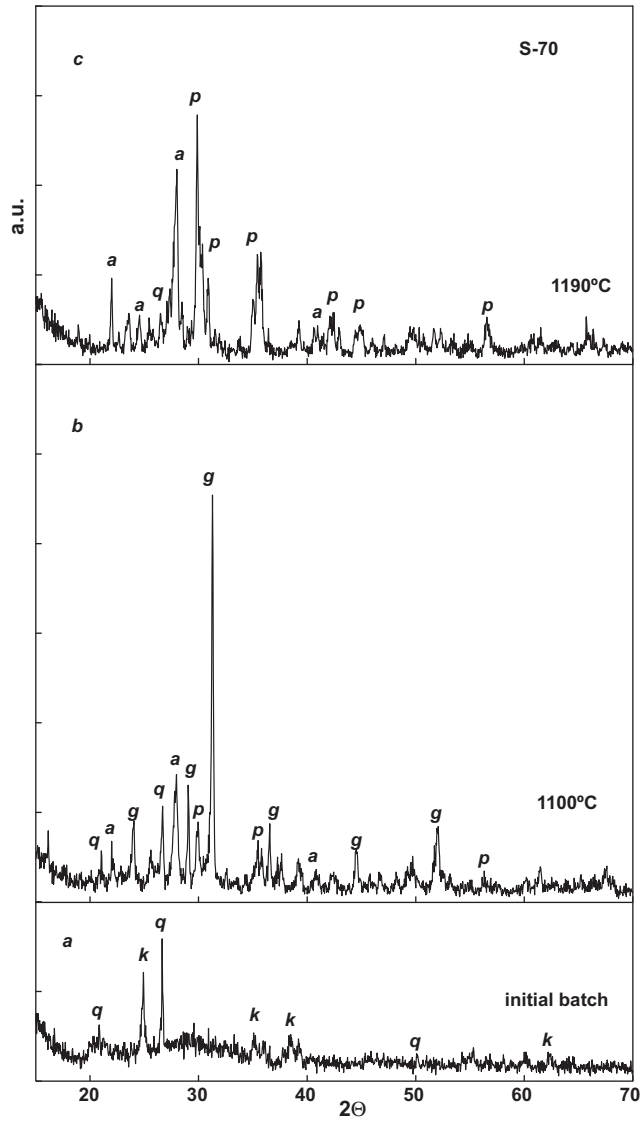

Fig. 7. XRD spectra of S-70 compositions after 30 min holding at different temperatures (q, quartz; a, anorthite; p, pyroxene; c, cristobalite; g, gehlenite; k, kailonite).

3.2. Phase formation

The main phase transformations in ceramic S-30, going on at different temperatures, are elucidated in Fig. 6, where XRD spectra of initial batch (a) and samples, obtained after 30 min at 1150 (b) and 1210 °C (c), respectively, are shown. The initial batch presents mainly quartz and kaolinite. The sample treated at 1150 °C demonstrates a small decreasing in the amount of quartz, as well as traces of gehlenite (due to crystallization of the amorphous slag) and traces of pyroxene and anorthite. At 1210 °C the decreasing of quartz phase is significant, the gehlenite phase totally disappears, while the amount of anorthite increases; traces of cristobalite are also observed.

These results are in agreement with the DTA and dilatometric ones and demonstrate that the sintering range occurs at higher temperature than the melting temperatures of gehlenite. It is also highlighted that the increasing of melt amount, which governs the densification process, is mainly related to the dissolution of quartz phase.

The phase transformations in ceramic S-70, which are summarised in Fig. 7, are quite different. The spectrum of parent batch (a) shows mainly amorphous halo (due to the huge amount of slag), kaolinite and low amount of quartz. At 1100 °C (b), because of crystallization of the slag, amorphous phase decreases and the main crystal phase becomes gehlenite; the beginning of anorthite and pyroxene formations are also identified. At 1190 °C (c) the gehlenite phase melts and entirely re-crystallises in pyroxenes and anorthite. Notwithstanding of the melting of gehlenite the sintering process at 1190 °C remains in its initial stag. This interesting fact can be explained by a rapid dissolution of SiO_2 and Al_2O_3 from the kaolin into slag melt, change of its composition and instantaneous crystallization into anorthite and pyroxene. This phase formation is identified by the exo-effect at 1170–1180 °C in Fig. 2.

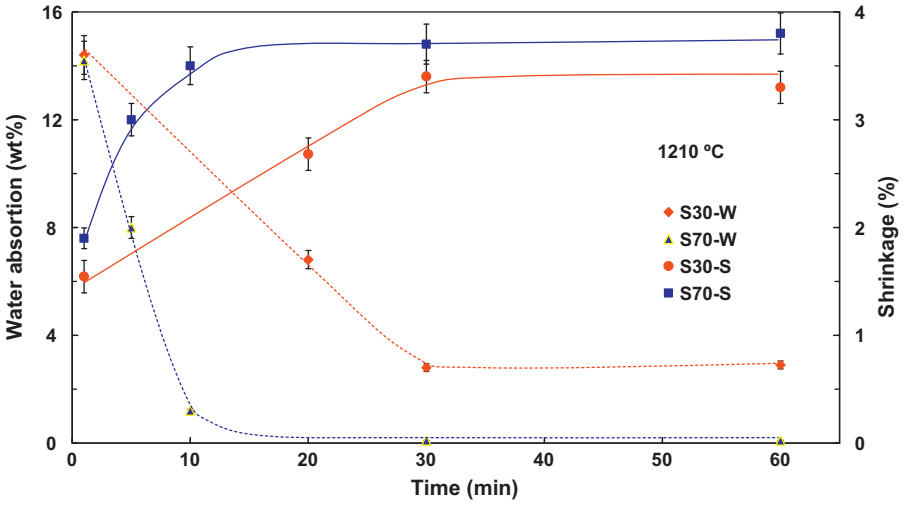

Fig. 8. Linear shrinkage and water absorption after different holding times at 210 °C.

The differences in sintering behaviours of S-30 and S-70 at 1210 °C were studied using samples, heat-treated for different times (between 1 and 60 min) at heating and cooling rates of 10 °C/min. The obtained results for the variations of water absorption and linear shrinkage are shown in Fig. 8.

After 1 min holding both compositions show a scarce degree of densification which points out that during heating the densification is insignificant. Afterwards the composition S-70 sinter rapidly and after 10–15 min the densification is completed: the obtained samples are characterised by zero water absorption and shrinkage of about 4%. At the same time, the sintering in S-30 finishes for 30–40 min but the samples remain with *W* of about 3%. This open porosity cannot be eliminated even after 3 h holding.

The peculiarities of phase formations, taking place during the sintering, were studied by XRD, using specimens which were rapidly quenched in air. The results for samples, quenched after 1 and 30 min holding at 1210 °C, as well as the spectrum of final ceramic (30 min holding at 1210 °C and cooling at 10 °C/min) are presented in Figs. 9 and 10 for ceramics S-30 and S-70, respectively.

The comparison of spectra 9-a and 9-b elucidate that during the sintering of ceramic S-30 a considerable dissolution of quartz carries out, as well as crystallization of anorthite and some cristobalite. The silica enrichment of the melt and the related viscosity rise can explain the lower sintering rate in this ceramic, while the subsequent formation of anorthite might elucidate the lower degree of densification and the residual open porosity. The spectrum of final ceramic is similar to one, obtained after quenching, which highlight that in S-30 no crystallization takes place during the cooling step.

The XRD results of S-70 show that the spectra of quenched samples after 1 and 30 min holding are similar, whereas one of cooled sample (10-c) is characterised by a higher crystallinity. This indicates that the melting of gehlenite, the dissolution of SiO_2 and Al_2O_3 from kaolin, the formation of pyroxene and anorthite and their partial melting carried out rapidly. This means that the viscosity of melt is relatively low, which explains the

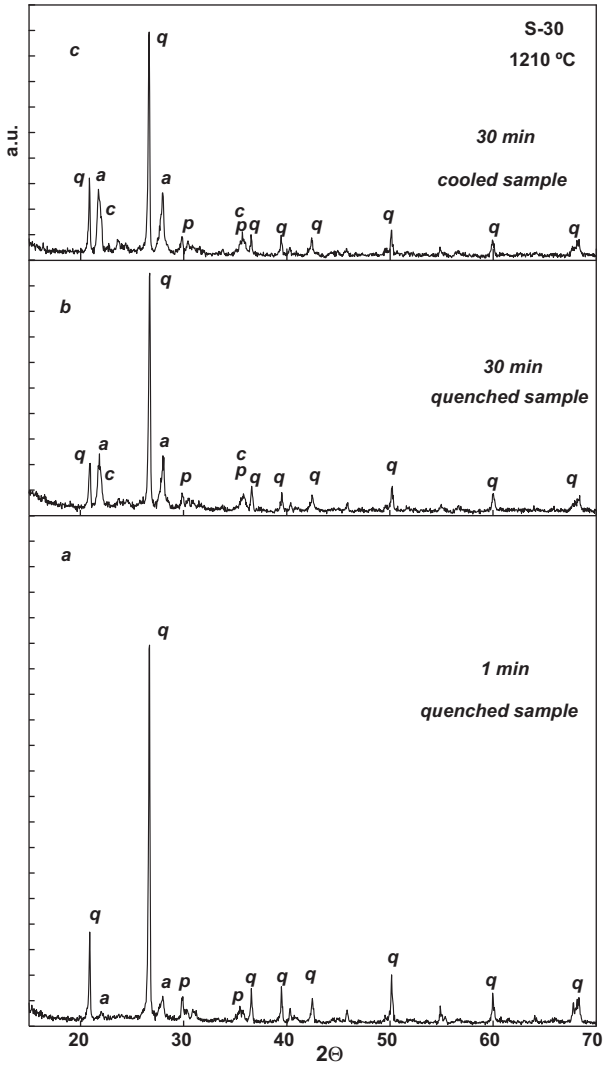

Fig. 9. XRD spectra of quenched and cooled S-30 samples after holding at 210 °C (q, quartz; a, anorthite; p, pyroxene; c, cristobalite).

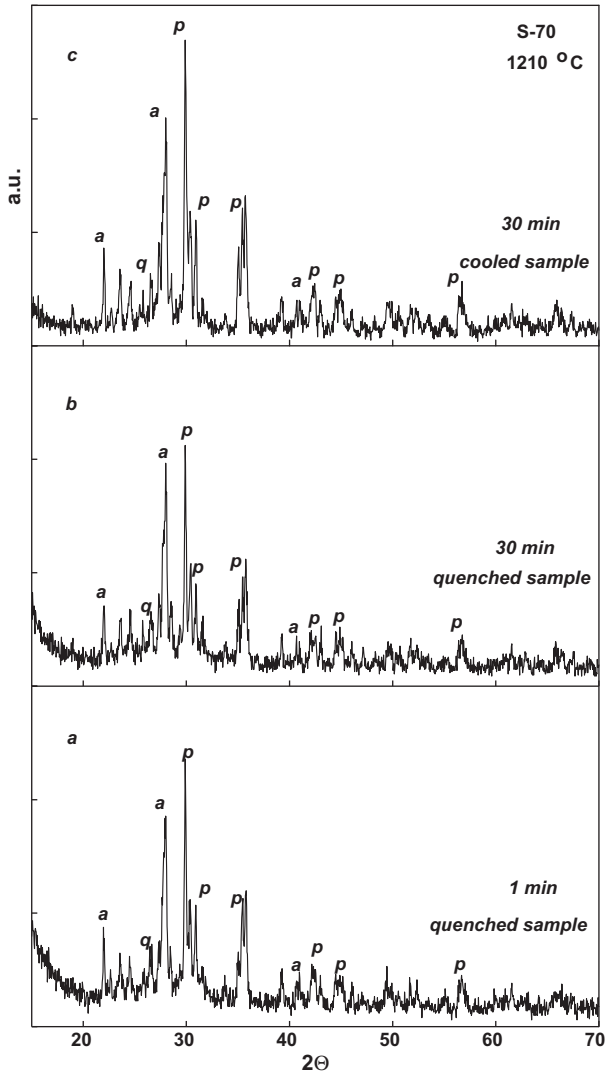

Fig. 10. XRD spectra of quenched and cooled S-70 samples after holding at 210 °C (q, quartz; a, anorthite; p, pyroxene).

short sintering time and the formation of new pyroxene phase during cooling.

An interesting peculiarity of any crystallization processes is the volume change, accompanying the phase transformation. It can lead to some crystallization shrinkage or/and to formation of crystallization induced porosity. This additional porosity was elucidated in different sintered glass-ceramics, forming pyroxenes,[27] as well as in a sintered material by milled basalitic tuffs.[28] It was supposed that similar phenomena take place also in some of the studied compositions.

In order to evaluate the formation of open and closed porosity in S-30 and S-70 ceramics the apparent, skeleton and absolute densities of cooled and quenched samples, treated for 30 min 1210 °C, were measured. The density results, together with the calculated values of closed and open porosities are summarised in Table 3.

The densities and porosities of both S-30 samples are similar, which verify the absence of phase formation or sintering during the cooling. The value of ∼7% open porosity is in a good agreement with obtained water absorption of ∼ 3%.

Table 3
Densities and porosities in quenched (Q) and cooled (C) S-30 and S-70 samples after 30 min heat-treatment at 1210 °C.

	Apparent density (g/cm^3)	Skeleton density (g/cm^3)	Absolute density (g/cm^3)	Open porosity (%)	Closed porosity (%)
S-30 Q	2.32	2.51	2.61	7.3	3.8
S-30 C	2.34	2.52	2.61	6.9	3.5
S-70 Q	2.12	2.14	2.86	0.7	25.2
S-70 C	2.13	2.15	2.95	0.6	28.6

In samples S-70 all values of apparent and skeleton densities are similar, which confirms the zero water absorption and demonstrate that no densification carries out during the cooling. At the same time, due to the supplementary crystallization during cooling, absolute density in the cooled sample increases with ∼0.1 g/cm^3, which leads to formation of additional 3–4% closed crystallization induced porosity.

The closed porosity in this ceramic is excessively high even in the quenched sample (∼25%), which probably is related to the slag crystallization and the presence of sulphur oxides. Similar "unusually" high closed porosities were observed also in other ceramics with high amount of wastes in the batch.[29] In order to elucidate these events additional experiments can be made.

3.3. Structure and properties

The structures of ceramics, obtained after 30 min at 1210 °C, were observed by SEM. Fig. 11 demonstrates the differences in surfaces of samples, while Fig. 12 elucidates the corresponding fractures.

The image of S-30 surface shows an uncompleted densification and some open pores, mainly with irregular shape and size of 10–30 μm, whereas ceramics S-50 and S-70 are characterised with well sintered and smooth surfaces and negligible porosity.

The image of S-30 fracture demonstrates open and closed pores, while the porosity in bulk of S-50 and S-70 practically is only closed. Some of the pores have size bigger than 70–100 μm, which elucidates some overfiring.

The fractures of ceramics S-30 and S-50, as well as the surfaces of pores are smooth, while ones of S-70 are rough and polycrystalline. In addition, tiny pores with 3–5 μm size, which might be associated with the crystallization during cooling, are observed in sample S-70. Fig. 13 shows typical closed pores, formed in S-50 (a) and S-70 (b), as well as a small crystallization induced pore in S-70 (c) with hexagonal crystals, identified by EDS analysis as anorthite.

The SEM-EDS observations of S-30 fracture elucidate the presence of residual quartz (Fig. 14-a) and some zones with a composition comparable to one of the kaolinite, where crystal structures similar to primary mullite are observed (Fig. 14-b).[30] According to the phase diagram, mullite cannot be formed in the new ceramics (see Fig. 1). For this reason, the presence of "nests

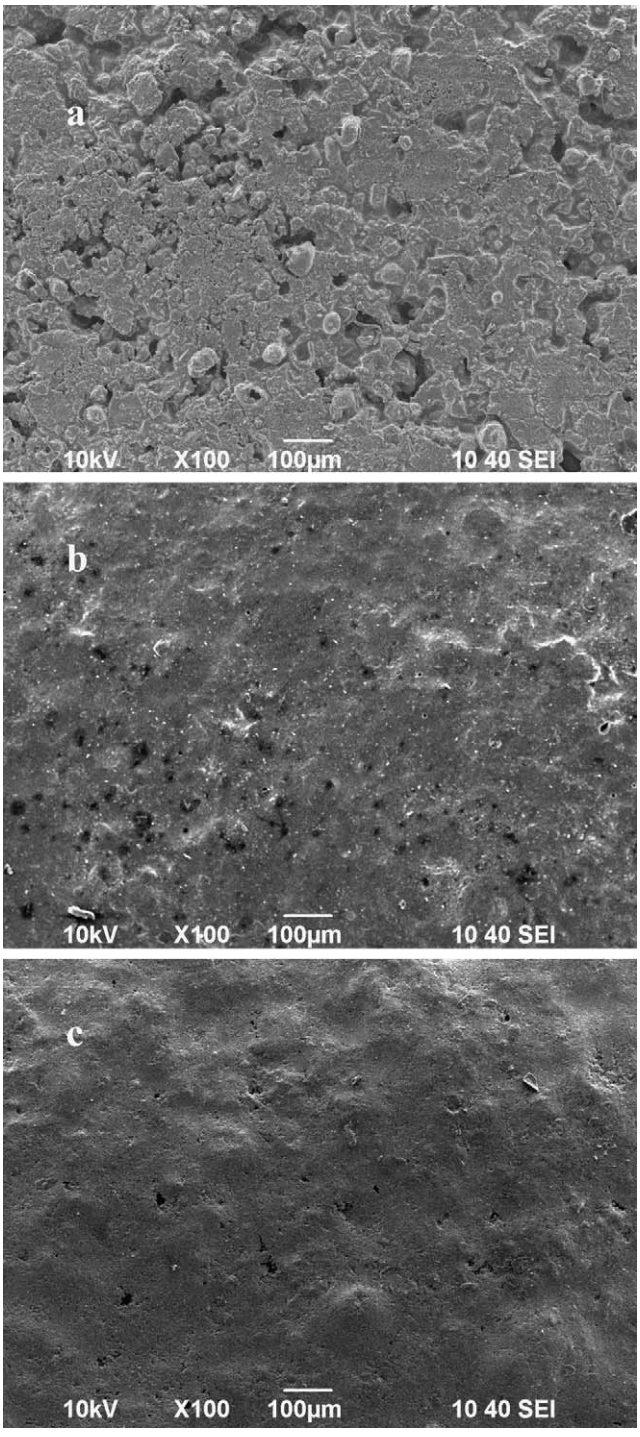

Fig. 11. SEM images of surface in samples S-30 (a), S-50 (b) and S-70 (c) after 30 min holding at 1210 °C.

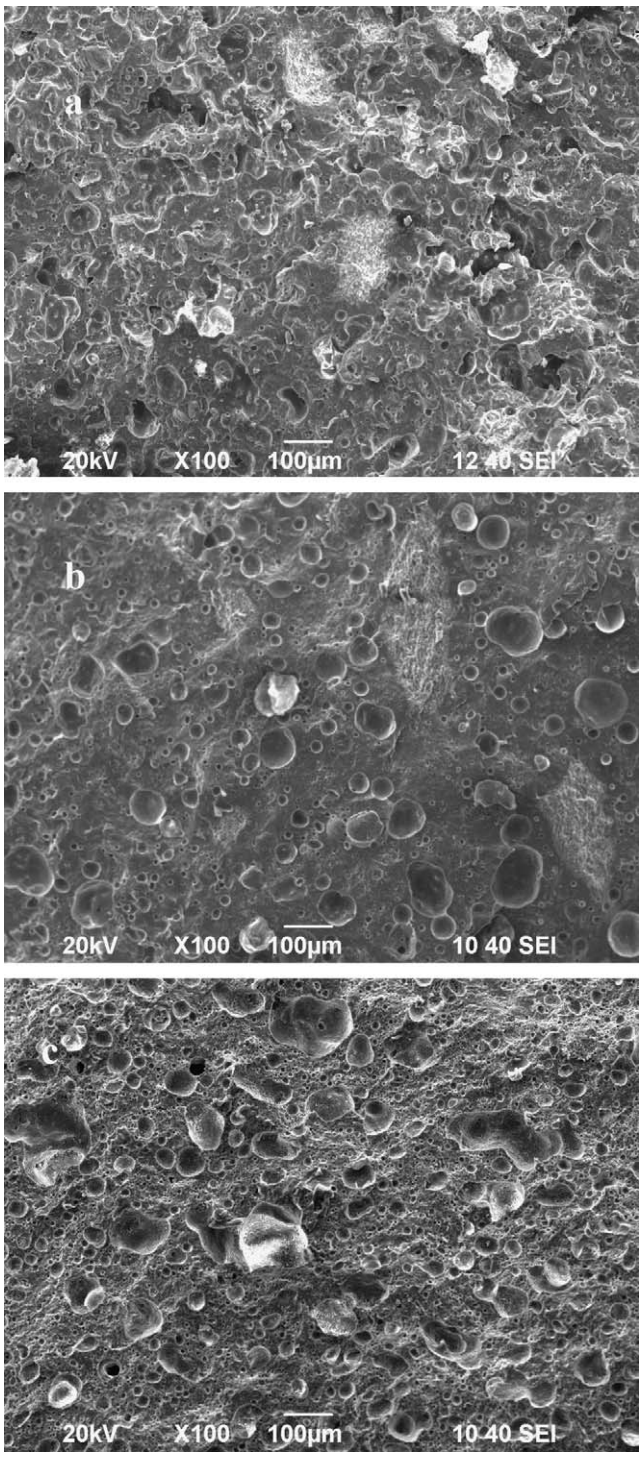

Fig. 12. SEM images of fractures in samples S-30 (a), S-50 (b) and S-70 (c) after 30 min holding at 1210 °C.

of primary mullite" can be related to an insufficient degree of homogenisation and to the short heat-treatment times. Similar targets absent in S-70 but were observed in S-50.

It can be also noted that, notwithstanding of 30 wt.% kaolin in the batches, the made XRD analyses do not distinguish the presence of mullite. In fact, due to overlapping with the peaks of quartz and other phases, the identification of low amount of this phase is quite difficult. Even in traditional ceramics, where only quartz and mullite are formed, the XRD evaluation of mullite requires serious and accurate studies.[31]

The measured properties of final ceramics are summarised in Table 4. The characteristics are similar or superior to these of the traditional earthenware tiles, which is a very positive initial result. However, it can be noted that the reproducibility of results is acceptable only for composition S-30 and partially for S-70. In S-50 the sintering interval is so narrow that it was

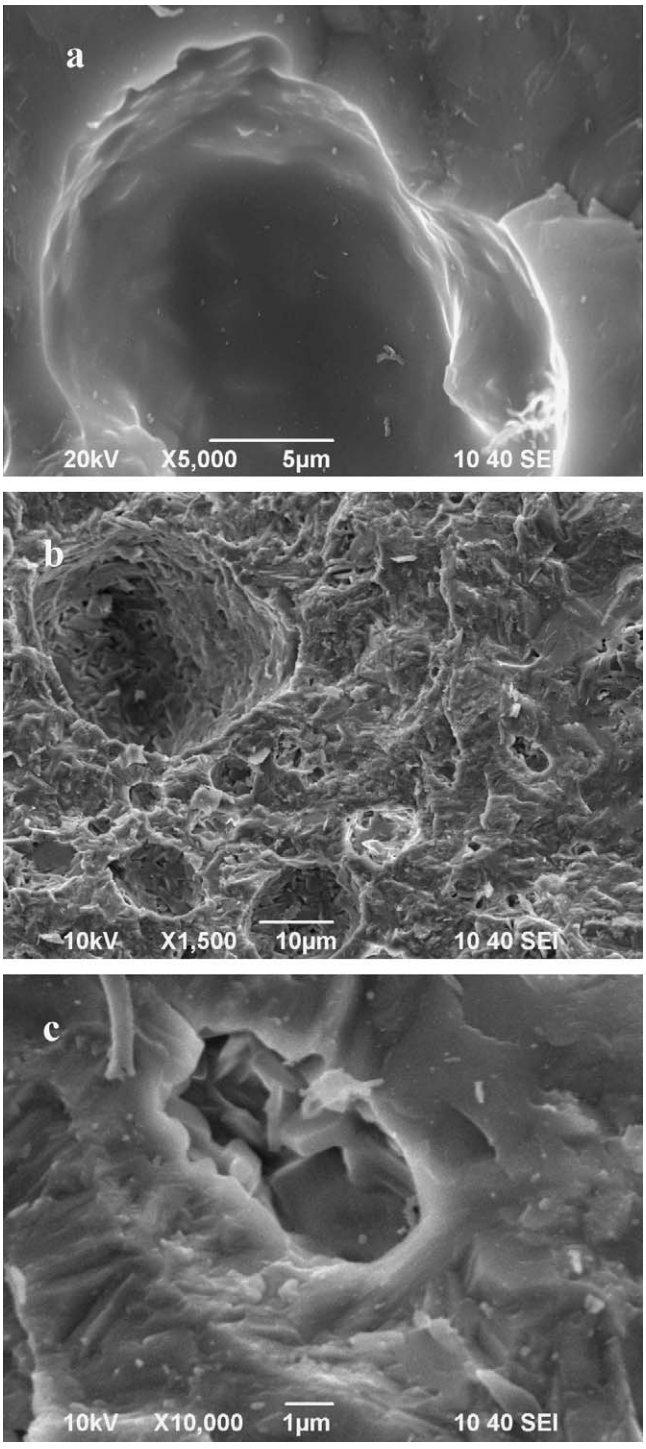

Fig. 13. SEM images of porosity in samples S-50 (a) and S-70 (b) and crystallization induced porosity in S-70 (c) after 30 min holding at 1210 °C.

Table 4
Properties of the new materials after 30 min heat-treatment at 1210 °C.

	Bending strength (MPa)	Vickers hardness (HV)	Apparent density (g/cm^3)
S-30	39 ± 2	550	2.34 ± 0.02
S-50	37 ± 7	624	2.22 ± 0.08
S-70	49 ± 4	830	2.13 ± 0.03

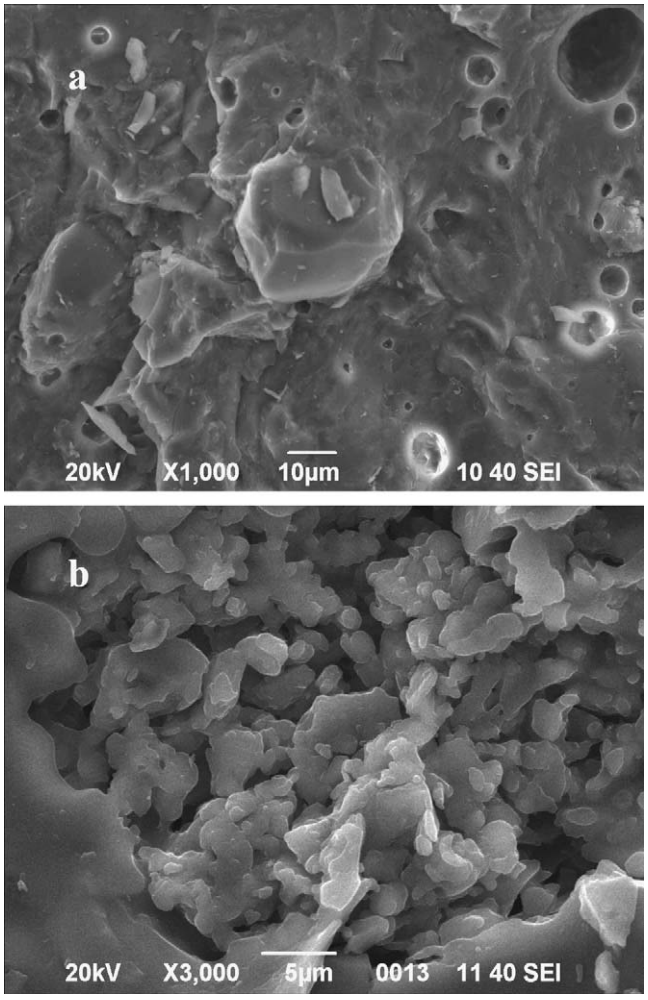

Fig. 14. SEM images of residual quartz (a) and crystal structures, similar to primary mullite (b) in ceramic S-30.

difficult to obtained samples with a uniform degree of sintering.

The hardness and the bending strength increase with slag amount in the batches. Notwithstanding of the lowest apparent density and the high closed porosity ceramic S-70 shows the best results, which can be related to its fine-crystalline structure and to the additional crystallization during cooling. An eventual decreasing of porosity in similar materials can lead to additional improvement of the mechanical characteristics.

4. Conclusion

New low-cost ceramics, with no traditional fluxes and 30, 50 and 70% blast furnace slag were synthesized at sintering temperatures of 1200–1220 °C. The obtained samples have good degrees of sintering and mechanical properties, which surpass ones of the conventional building and tiling materials.

The final phase compositions of studied ceramics are in agreement with the phase diagrams and are totally different by ones of the traditional ceramics: the samples are characterized by an elevate crystallinity and formation of anorthite solid solutions and pyroxenes.

Acknowledgments

The authors gratefully acknowledge the financial support within Project TK-X-1713/07 (Bulgarian Ministry of Science and Education).

References

1. Gennaro R, Cappelletti P, Cerri G, Gennaro M, Dondi M, Guarini G, et al. Influence of zeolites on the sintering and technological properties of porcelain stoneware tiles. *J Eur Ceram Soc* 2003;**23**:2237–45.
2. Carbonchi G, Dondi M, Morandi N, Tateo F. Possible use of altered volcanic ash in ceramic tile production. *Ind Ceram* 1999;**19**:67–74.
3. Ergul S, Akyildiz M, Karamanov A. Ceramic material from basaltic tuffs. *Ind Ceram* 2007;**37**:75–80.
4. Kurama S, Kara A, Kurama H. The effect of boron waste in phase and microstructural development of a terracotta body during firing. *J Eur Ceram Soc* 2006;**26**:755–60.
5. Asquini L, Furlani E, Bruckner S, Maschio S. Production and characterization of sintered ceramics from paper mill sludge and glass cullet. *Chemosphere* 2008;**71**:83–9.
6. Bragança SR, Licenzi J, Guerino K, Bergmann CP. Recycling of iron foundry sand and glass waste as raw material for production of whiteware. *Waste Manage Res* 2006;**24**:60–6.
7. Matteucci F, Dondi M, Guarini G. Effect of soda-lime glass on sintering and technological properties of porcelain stoneware tiles. *Ceram Int* 2002;**28**:873–80.
8. Tucci A, Esposito L, Rastelli E, Palmonari C, Rambaldi E. Use of soda-lime scrap-glass as a fluxing agent in a porcelain stoneware tile mix. *J Eur Ceram Soc* 2004;**24**:83–92.
9. Andreola F, Barbieri L, Karamanova E, Lancellotti I, Pelino M. Recycling of CRT panel glass as fluxing agent in the porcelain stoneware tile production. *Ceram Int* 2008;**34**:1289–95.
10. Raimondo M, Zanelli C, Matteucci F, Guarini G, Dondi M, Labrincha JA. Effect of waste glass (TV/PC cathodic tube and screen) on technological properties and sintering behaviour of porcelain stoneware tiles. *Ceram Int* 2007;**33**:615–21.
11. Dana K, Das SK. Partial substitution of feldspar by B.F. slag in triaxial porcelain: Phase and microstructural evolution. *J Eur Ceram Soc* 2004;**24**:3833–9.
12. Ghosh S, Das M, Chakrabarti S, Ghatak S. Development of ceramic tiles from common clay and blast furnace slag. *Ceram Int* 2002;**28**:393–400.
13. Osipov VA, Timofeeva ZG, Kurbatskii MN, Mironova PV, Ocheretnyuk FF. Blast furnace granulated slag in the production of building ceramicss. *Glass Ceram* 1990;**47**:228–30.
14. Ozdemir I, Yilmaz S. Processing of unglazed ceramic tiles from blast furnace slag. *J Mater Process Technol* 2007;**183**:13–7.
15. Andreola F, Barbieri L, Corradi A, Lancellotti I, Manfredini T. Utilisation of municipal incinerator grate slag for manufacturing of porcelainized stoneware tiles manufacturing. *J Eur Ceram Soc* 2002;**22**: 1457–62.
16. Barbieri L, Corradi A, Lancellotti I, Manfredini T. Use of municipal incinerator bottom ash as sintering promoter in industrial ceramics. *Waste Manage* 2002;**22**:859–63.
17. Acosta A, Iglesias I, Aineto M, Romero M, Rincon JM. Utilisation of IGCC slag and clay steriles in soft mud bricks (by pressing) for use in building bricks manufacturing. *Waste Manage* 2002;**22**:887–91.
18. Aineto M, Acosta A, Iglesias I. The role of a coal gasification fly ash as clay additive in building ceramic. *J Eur Ceram Soc* 2006;**26**:3783–7.
19. Chandra N, Sharma P, Pashkov GL, Voskresenskaya EN, Amritphale SS, Baghel NS. Coal fly ash utilization: low temperature sintering of wall tiles. *Waste Manage* 2008;**28**:1993–2002.
20. Zimmer A, Bergmann CP. Fly ash of mineral coal as ceramic tiles raw material. *Waste Manage* 2007;**27**:59–68.
21. Diaz LA, Torrecillas R. Porcelain stoneware obtained from the residual mud of serpentinuite raw materials. *J Eur Ceram Soc* 2007;**27**:2341–5.
22. Torres P, Manjate RS, Quaresma S, Fernandes HR, Ferreira JMF. Development of ceramic floor tile compositions based on quartzite and granite sludges. *J Eur Ceram Soc* 2007;**27**:4649–55.
23. Colombo P, Brusatin G, Bernardo E, Scarinci G. Inertization and reuse of waste materials by vitrification and fabrication of glass-based products. *Curr Opin Solid State Mater* 2003;**7**:225–39.
24. Rawlings RD, Wu JP, Boccaccini AR. Glass-ceramics: their production from wastes-a review. *J Mater Sci* 2006;**41**:733–61.
25. Osborn EF, DeVries RC, Gee K, Kraner H. Optimum composition of blast furnace slag as deduced from system SiO_2–Al_2O_3–CaO–MgO. *Trans Am Inst Min Mettall Pet Eng* 1954;**20**:33–45.
26. Karamanova E, Avdeev G, Penkov I, Karamanov A. Sintering and phase formation in ceramic materials from blast furnace slag. In: *Proceedings of the 8th Int. Conf. SGEM'2008*. 2008. p. 789–96.
27. Karamanov A, Pelino M. Induced crystallization porosity and properties of sintered diopside and wollastonite glass-ceramics. *J Eur Ceram Soc* 2008;**28**:555–62.
28. Karamanov A, Arrizza L, Ergul S. Sintered material from alkaline basaltic tuffs. *J Eur Ceram Soc* 2009;**29**:595–601.
29. Karamanova E, Karamanov A, Andreola F, Barbieri L, Lancellotti I, Schabbach LM. Sintering study of new ceramic materials based on incinerator secondary raw material and refractory clay. In: *Proceedings of the IIth Int. Conf. Hazardous and Industrial Waste Management*. 2010.
30. Lee WE, Souza GP, McConville CJ, Tarvornpanich T, Iqbal Y. Mullite formation in clays and clay-derived vitreous ceramics. *J Eur Ceram Soc* 2008;**28**:465–71.
31. Martin-Marquez J, De la Torre AG, Aranda MAG, Rincon JM, Romero M. Evolution with temperature of crystalline and amorphous phases in porcelain stoneware. *J Am Ceram Soc* 2009;**92**:229–34.